Performance Analysis of Different Slot Waveguide Structures for Evanescent Field Based Gas Sensor Applications

VEER CHANDRA (veer.ecpg16@nitp.ac.in)
National Institute of Technology Patna https://orcid.org/0000-0003-4159-0169
Rakesh Ranjan
National Institute of Technology Patna

Research Article

Keywords: Slot waveguide, Sensitivity, Evanescent field, Propagation loss, Methane gas.

Posted Date: March 30th, 2021

DOI: https://doi.org/10.21203/rs.3.rs-344243/v1

Version of Record: A version of this preprint was published at Optical and Quantum Electronics on August 6th, 2021. See the published version at https://doi.org/10.1007/s11082-021-03102-8.

Performance Analysis of Different Slot Waveguide Structures for Evanescent Field based Gas Sensor Applications

Veer Chandra and Rakesh Ranjan
OFC and Photonics Research lab,
Department of Electronics and Communication Engineering,
National Institute of Technology Patna, India.
*E-mail: veer.ecpg16@nitp.ac.in

Abstract. Slot waveguide has emerged as a potential candidate for the design of evanescent field absorption based photonic gas sensors, optical quantum information applications, etc. In this paper, three different slot waveguide structures, i.e., conventional slot, partial-strip-loaded slot, and full-strip-loaded slot waveguides have been explored to analyze their sensing performance for the methane gas. As the methane gas has the peak absorption at around 3.31 μm, therefore, this has been considered as the operating wavelength for the analysis. In anticipation of improvement in evanescent field ratio in slot region and hence, the sensing capabilities of the gas sensor, the slot waveguide structures have been designed by depositing the germanium layer over the calcium fluoride in different manners. To realize the significant evanescent field and sensitivity along with relatively low propagation loss, the suitable dimension of the slot waveguide structures has been chosen very judiciously. Several waveguide parameters, such as evanescent field ratio, propagation loss, and sensitivity have been chosen for the analysis and comparison of slot waveguide structures, by varying the arm-width and thickness of germanium layer. Simulation results have demonstrated that the full-strip-loaded slot waveguide has the superior performance in terms of higher evanescent field and higher sensitivity, which is followed by the partial-strip-loaded slot waveguide, even for the fixed target value of propagation loss. Moreover, the current analysis may be extended for the design of suitable photodetector that can further enhance the performance of the gas sensor.

Keywords: Slot waveguide; Sensitivity; Evanescent field; Propagation loss; Methane gas.

1. Introduction

The photonic waveguide based sensor applications are very popular due to its low cost, ultra-compact size, high sensitivity, easy to fabricate, and CMOS compatibility (Bogaerts et al. 2005), which can be used in various applications, such as bio-medical, chemical detection, gas detection, etc. Usually, the absorption property based photonic sensing approach is preferred over the effective index based sensing. In presence of the material/sample taken for sensing, the change in the effective index is quite smaller than change in the evanescent field, which is mainly due to the absorption of light by the sensing material (Butt et al. 2017; Ranacher et al. 2018). The extent of light absorption depends on the dimension/material of sensor device, the operating wavelength, and the material to be sensed. The authors in (Ranacher et al. 2018; Datta et al. 2021; Cherouana et al. 2019) have presented the idea of an evanescent field based photonic gas sensor using different types of photonic waveguides, namely strip, rib, and slot in the mid-infrared region. The percentage of evanescent field/light in upper cladding/slot region of the photonic waveguide changes during its interaction with the molecules of the sensing material. Therefore, the photonic sensors are required to be designed with the waveguides having comparatively larger evanescent field in the upper cladding region. The authors in (Butt et al. 2017; Huang et al. 2014) have demonstrated that the slot waveguide has the highest EFR (Evanescent Field Ratio) in the slot (upper cladding) region than the other photonic waveguide structures, which comes at the cost of higher propagation loss (Ding et al. 2010; Almeida et al. 2004; Debnath et at. 2016; Rifat et al. 2019). In the slot waveguide, the light is mostly confined in the slot region, therefore, it has reasonably higher evanescent field value (Soref et al. 2006; Tien et al. 2010; Baehr-Jones et al. 2010; Li et al. 2011; Xu et al. 2020; Nacer et al. 2020; Parriaux et al. 1998). Moreover, to compensate the propagation loss, a light source of comparatively high input power may be used. Since, the sensitivity of the photonic sensor is mainly dependent on the percentage of evanescent field/light in the upper cladding region; therefore, it can be anticipated that slot waveguide can offer significantly higher sensitivity than the other photonic waveguide structures.

The current work explores the possibilities of different slot waveguide structures, designed with germanium (Ge) and calcium fluoride (CaF_2) materials, for gas sensor applications. In this analysis, two important waveguide parameters, evanescent field and propagation loss have been investigated in order to determine the sensitivity of the gas sensor. As the peak absorption of methane gas is in the mid-infrared region, near around 3.31 μm; therefore, for the current analysis the operating wavelength has been considered as 3.31 μm.

The authors in (Kai-he et al. 2019) have presented the analysis of Si-SiO_2 (SOI) based methane gas sensor using the slot micro-ring resonator structure. Moreover, beyond 3.6 µm of wavelength, the SiO_2 material becomes highly absorbing; and hence, the SOI based waveguides cannot be used in this range of mid-IR region. Therefore, the materials having the wide transparency range in mid-IR region (Mere et al. 2016; Soref 2010; kimet al. 2018), along with high-index contrast, like germanium and calcium fluoride, can be suitably used for methane gas sensing applications than SOI materials. The gas sensor analysis for different gases have been provided in (Dong et al. 2017; Zheng et al. 2017; Rouxel et al. 2015; Fabricius et al. 1992; Yebo et al. 2010).
The outline of the paper is as follows. Section II presents the design structures of different slot waveguides and its parameters, which is followed by the simulation results in terms of different waveguide parameters in Section III. The comparison and performance analysis of all the three slot waveguide structures have been presented in Section IV. Finally, the work has been concluded in Section V.

2. Waveguide structures and parameters

2.1 Design of waveguide

The cross sectional view of three different structures of Ge-on-CaF_2 materials based slot waveguides have been presented in Fig. 1, where '*W*' is the arm width (Ge), '*H*' is the total height of the germanium layer, '*t*' is the thickness of Ge-layer developed above the CaF_2, and '*G*' is the slot gap of the slot waveguides. The conventional slot waveguide has been depicted in Fig. 1 **a**, whereas, the partial-strip-loaded and full-strip-loaded slot waveguides have been shown in Figs. 1 **b** and **c**.

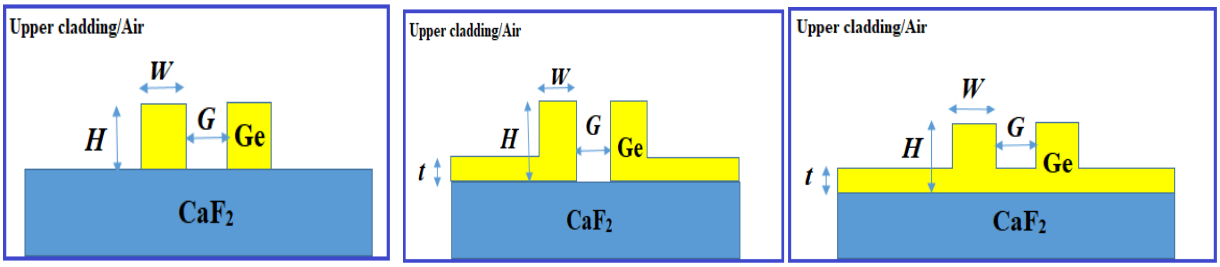

a **b** **c**

Fig. 1 Structures of three different slot waveguides using Ge-on-CaF_2 materials **a** conventional slot waveguide, **b** partial-strip-loaded slot, and **c** full-strip-loaded slot.

The material used for the lower cladding layer is CaF_2, having the refractive index of 1.40 and the layers developed above the CaF_2, are using the Ge material, having the refractive index of 4.02 at the operating wavelength of 3.31 µm. In slot waveguide, the evanescent field in the slot region is the quasi-TE mode only. Further, to get the stronger evanescent field in slot region, the slot waveguide with smaller dimension is desirable. With the decrease in arm widths, the amount of evanescent field increases, which leads to better sensing capabilities (Katti et al. 2018). However, further decrement in arm width may cause the leakage of the quasi-TE mode and it may no longer remain as a guiding mode (Huang et al. 2016). Therefore, it is essential to investigate the suitable waveguide dimension for all the considered slot waveguide structures for the effective propagation of quasi-TE mode. Out of the three slot waveguide structures presented in the current work, the partial-strip-loaded, and full-strip-loaded slot waveguides have been developed respectively by depositing a thin Ge-layer, partially and fully, on CaF_2 material, as depicted in Figure 1, in anticipation of further enhancement of evanescent field in the slot region. Here, it is assumed that the upper cladding region is surrounded by the air or gas to be sensed.

2.2 Evanescent field ratio (EFR)

The evanescent field ratio is a crucial parameter for the realization of evanescent field absorption based devices/sensors. The evanescent field ratio is defined as the amount of power in upper cladding/slot region, interacting with the environment/material to be sensed, to the total incident power on the device. The EFR mainly depends on the

geometry and operating wavelength of the photonic waveguide. Mathematically, the EFR can be expressed as (Chandra et al. 2020), in the Eq. (1) below,

$$\eta = \frac{\iint_{evan} \vec{S}.\vec{n}\, dx\, dy}{\iint_{Total} \vec{S}.\vec{n}\, dx\, dy} \tag{1}$$

where, η is the evanescent field ratio, $\vec{S}$ is the Pointing vector of the mode field in the waveguide and $\vec{n}$ is the normal vector to the waveguide cross-section.

2.3 Propagation loss

Besides the evanescent field ratio, the propagation loss in the waveguide plays a critical role to analyze the performance of the sensor designs. The waveguide propagation loss mainly depends on the waveguide geometries and it is highly reliant on the imaginary part of the effective refractive index, as expressed in Eq. (2) below (Du et al. 2013; Lindecrantz et al. 2014; Huang et al. 2016),

$$\text{Loss (dB)} = 10 \times \log_{10}(\text{e}) \times \frac{4\pi \times Im(n_{eff})}{\lambda} \tag{2}$$

2.4 Sensitivity

The photonic sensors are required to be designed with waveguides having comparatively high sensitivity. The sensitivity can be estimated by the Eq. (3) (Butt et al. 2017; Huang et al. 2014) below,

$$Sensitivity(s) = -\eta\varepsilon L \exp(-\eta\varepsilon C L - \alpha_{wvg} L) \tag{3}$$

where $\eta, \varepsilon, C, \alpha_{wvg}$, and L are the evanescent field ratio, absorption coefficient, concentration, intrinsic waveguide loss, and length of the waveguide, respectively. Hence, the sensitivity of a photonic device is highly dependent on EFR (η) and concentration (C) of the material to be sensed. Further, the optimum length (L_{opt}) is a waveguide length at which the sensitivity is maximum and beyond that the sensitivity starts to decay due to waveguide loss. For a photonic sensor/device, it can be obtained by solving the equation, $\frac{ds}{dL} = 0$, from Eq. (3) above. Therefore, the optimum length can be expressed, as noted in Eq. (4) below,

$$L_{opt} = \frac{1}{\eta\varepsilon C + \alpha_{wvg} L} \tag{4}$$

where, $Im(n_{eff})$ is the imaginary part of the effective refractive index, and λ is the operating wavelength. From Eq. (2), it is clear that for a fixed operating wavelength, the propagation length varies only with $Im(n_{eff})$.

3. Simulation Results

The simulation analysis has been performed using the finite element method (FEM) based COMSOL Multiphysics simulation platform. During the simulation, the scattering boundary condition has been applied, in order to address the propagation loss for all the three considered slot waveguide structures.

3.1 Mode field distribution

For all the three types of slot waveguide structures, the mode field distributions have been illustrated in Figs. 2, 3, and 4 respectively. Fig. 2 shows the mode field distribution and corresponding normalized electric field distribution for the conventional slot waveguide, where, W = 0.55 µm, G = 80 nm, and H = 0.50 µm. The figures clearly depict that the light is mostly confined in the slot region of the waveguide, which is mainly due to the discontinuity of electric field in high refractive index regions (Lio et al. 2015; Verma et al. 2017) (i.e., Ge); whereas, the optical field intensity in high refractive index regions is extremely low. Further, with the other desired values of arm width (W) and gap (G), the similar mode field distributions have also been obtained that are used for the analysis of different waveguide parameters.

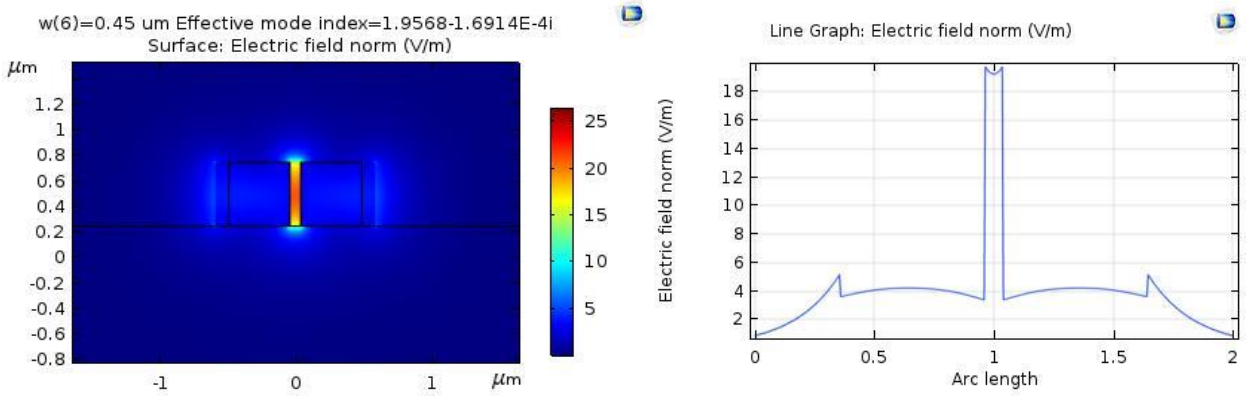

a **b**

Fig. 2 Mode field distribution for **a** conventional slot waveguide, and **b** plot of corresponding normalized electric field distribution at $W = 0.55$ µm, $G = 0.08$ µm, and $H = 0.50$ µm.

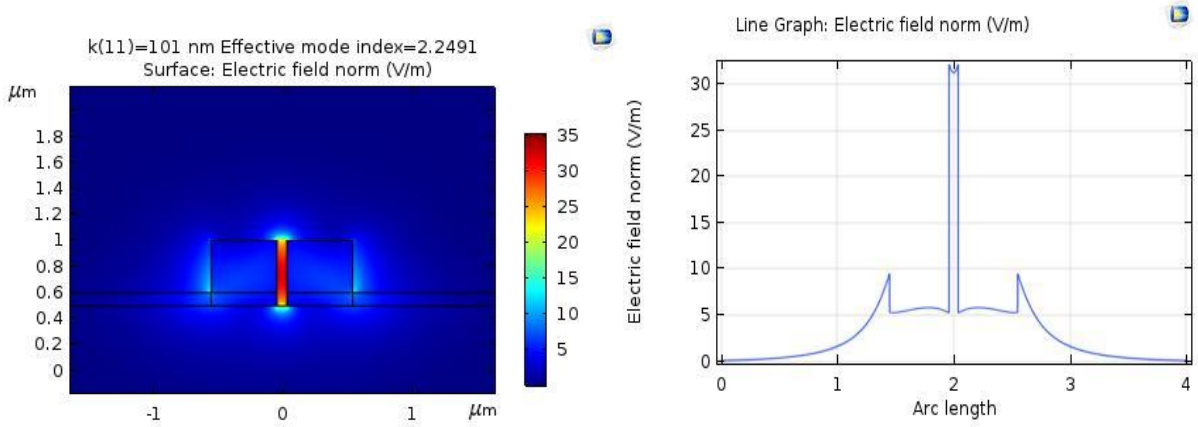

a **b**

Fig. 3 Mode field distribution for **a** partial-strip-loaded slot, and **b** plot of corresponding normalized electric field distribution (right) at $W = 0.51$ µm, $G = 80$ nm, $H = 0.5$ µm, and $t = 101$ nm

Likewise, Fig. 3 shows the mode field distribution and corresponding normalized electric field distribution for the partial-strip-loaded slot waveguide. Due to the development of additional layer of germanium, except in between the waveguide arms, over the lower cladding layer, of thickness '*t*', the light is more confined in the slot region of partial-strip-loaded slot waveguide, than the conventional slot waveguide. For the design of partial-strip-loaded slot waveguide, the comparable waveguide parameters have been considered, such as $W = 0.51$ µm, $G = 80$ nm, and $H = 0.50$ µm, and $t = 0.101$ µm. From the figure, it is apparent that the amplitude of the normalized electric field in the slot region is significantly larger than that recognized with conventional slot waveguide structure. Therefore, with the partial-strip-loaded slot waveguide, the higher evanescent field can be achieved, which is desirable to attain the high sensing performance.

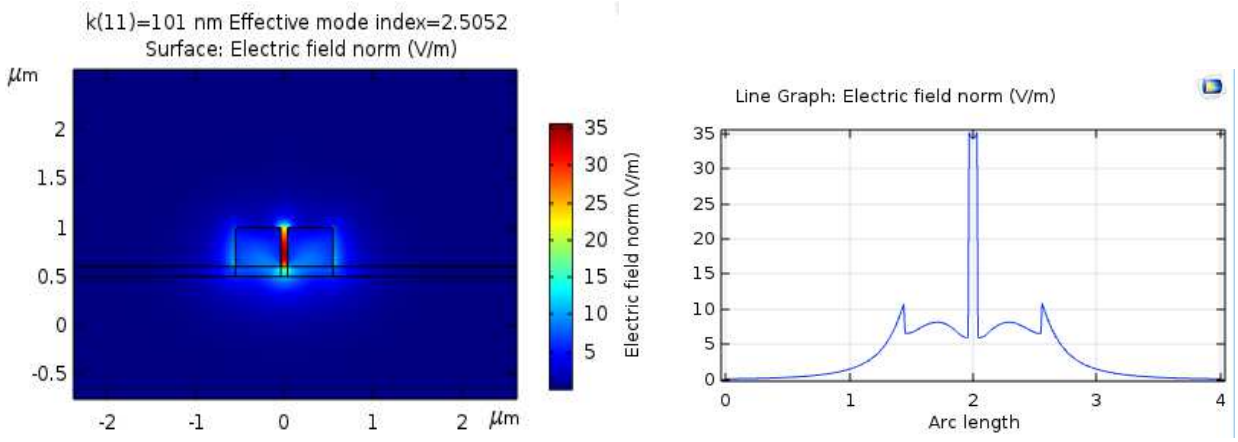

a **b**

Fig. 4 Mode field distribution **a** for full-strip-loaded slot, and **b** plot of corresponding normalized electric field distribution at W = 0.51 μm, G = 80 nm, H = 0.5 μm, and t = 101 nm.

Subsequently, the distributions of mode field and corresponding normalized electric field for the full-strip-loaded slot waveguide have been illustrated in Fig. 4. For this particular slot waveguide structure, a thin layer of germanium material has been deposited over the entire lower-cladding layer, including the slot region between the two arms. This structure offers the further improvement in mode field distribution as well as in electric field amplitude over the previous two slot waveguide structures. Therefore, by inserting a thin layer of germanium over the lower cladding layer, the high light confinement in slot region can be achieved, as observed with partial-strip-loaded and full-strip-loaded slot waveguide structures, as compared to the conventional slot waveguide.

3.2 Evanescent field ratio vs. waveguide dimension

It is well known that due to high EFR in slot region, the slot waveguide is one of the popular structure to realize the evanescent field based photonic sensor devices. The presence of amount of evanescent field in slot region is highly dependent on the appropriate choice of the waveguide structure and dimension; therefore, it is essential to visualize the impact of variations in waveguide dimension on EFR for all the three considered slot waveguide structures. For the conventional slot waveguide, the arm width (W) has been varied from 0.45 μm to 0.65 μm for two different slot gaps (G) of 80 nm and 120 nm, as depicted in Fig. 5 **a**. From the figure, it is clear that the percentage of evanescent field ratio first decreases with the increase in arm width. Moreover, for G = 80 nm, it has been observed that the evanescent field ratio increases abruptly at W = 0.51 μm and achieves the maximum EFR (of 30%) at around W = 0.52 μm. Before, W = 0.51 μm, the light confinement is mostly either in side arms (Ge) or in lower-cladding regions and from W = 0.51μm, the light starts propagating mainly through the slot region. Furthermore, after W = 0.52 μm, the light confinement in the slot region decreases gradually with the increase in arm widths. A similar observation has been made for G = 120 nm and light confinement in slot region starts with W = 0.53 μm, which attains the peak EFR (of 28%) at around W = 0.54 μm, before the start of gradual decrement of light confinement in slot region. Similarly, for the evanescent field analysis in partial-strip-loaded slot waveguide, and full-strip-loaded slot waveguide, the thickness (t) of Ge-layer has been varied from 0 to 140 nm, in order to search the optimal thickness of Ge-layer to achieve the maximum EFR in the slot region. Again, the two slot gaps of 80 nm, and 120 nm have been considered for the analysis and depicted in Figs. 5 **b** and **c** respectively for partial-strip-loaded and full-strip-loaded slot waveguide structures.

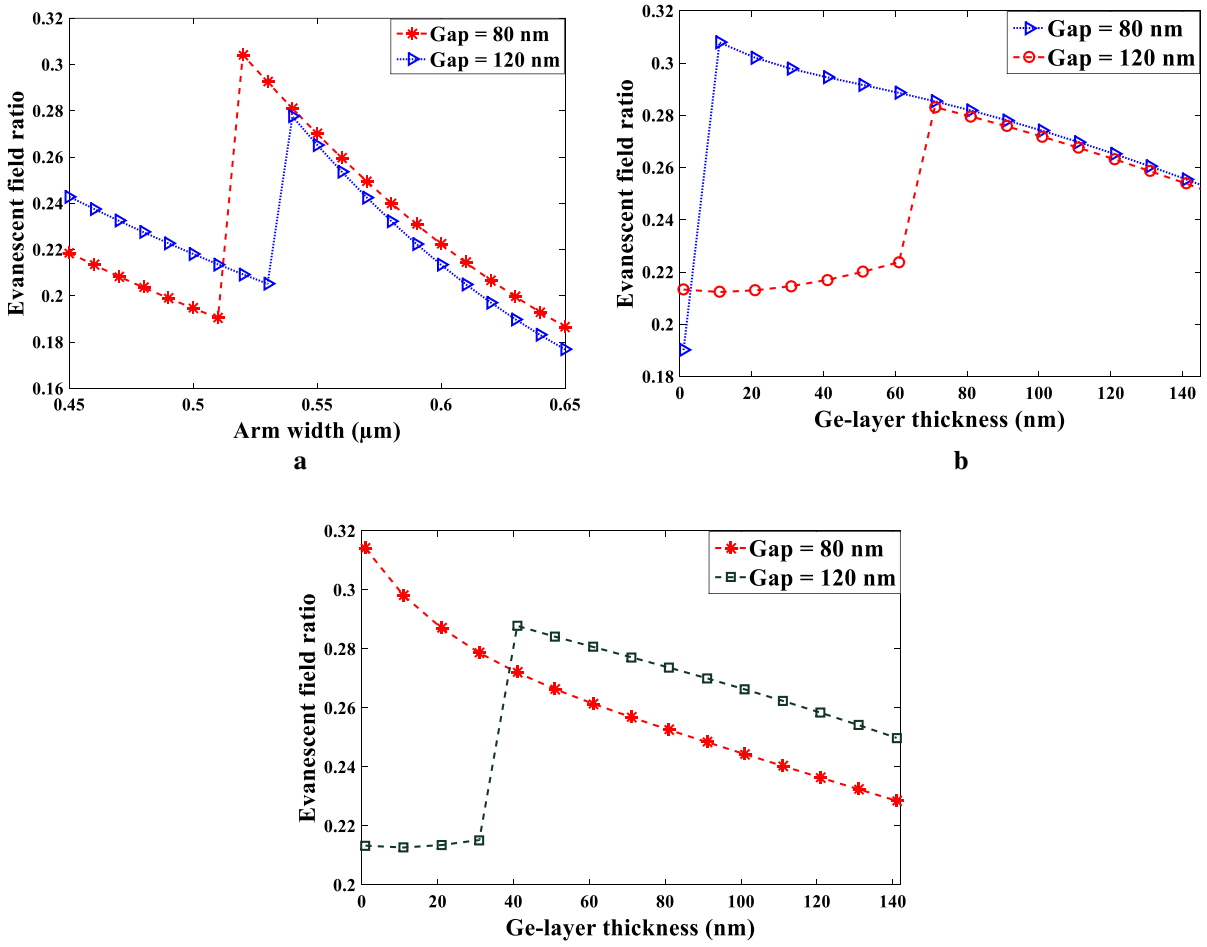

Fig. 5 Evanescent field ratio variations **a** with the arm width (*W*) at two different slot gaps (*G*) in Slot waveguide **b** with Ge-layer thickness (*t*) at two different slot gaps (*G*) in partial-strip-loaded slot, and **c** with Ge-layer thickness (*t*) at two different slot gaps (*G*) in full-strip-loaded slot waveguide.

Based on the previous analysis with conventional slot waveguide and from the meticulous simulations with partial-strip-loaded slot waveguide and full-strip-loaded slot waveguide, here, the arm width (*W*) for has been fixed around 0.51 μm. From Fig. 5 **b**, for partial-strip-loaded slot waveguide, the maximum level of evanescent field has been observed as ~30.22 % and ~28.31 % respectively for the slot gaps of 80 nm and 120 nm at their respective Ge-layer thicknesses (*t*) of 10 nm and 60 nm. Likewise, for full-strip-loaded slot waveguide, Fig. 5 **c** shows the variations in EFR with respect to Ge-layer thickness (*t*). The maximum EFR have been noted as ~31.4% and ~28.77% for the same respective slot gaps with its corresponding 't' values of 0 nm and 40 nm. After attaining the highest EFR values in both partial-strip-loaded and full-strip-loaded slot waveguide structures, the increase in '*t*' leads to decrease in EFR. Moreover, these obtained values of '*W*' and '*t*' for the considered slot waveguides are corresponding to the maximum EFR value in slot region. Nevertheless, along with the EFR, the propagation loss has significant impact to turn up with the optimal dimension of waveguides with higher sensitivity and lower propagation loss, which have been discussed in the subsequent sub-sections below.

3.3 Propagation loss vs. waveguide dimension

Propagation loss is mainly dependent on the materials used and geometry of the photonic waveguide. From the previous analysis, it can be anticipated that the deposition of Ge-layer on CaF_2 may results in decrement in propagation loss in the slot waveguide structures. To visualize the effect of variations in waveguide dimension on propagation loss, the arm width of the slot waveguide has been again varied from 0.45 μm to 0.65 μm for the two slot gaps of 80 nm and 120 nm. Using the simulation analysis, first the imaginary part of effective refractive index ($Im(n_{eff})$) has

been obtained. Further, utilizing these values of $Im(n_{eff})$ for different dimensions of slot waveguides in Eq. (2), the propagation loss in slot waveguides can be obtained. Figure 6 **a** illustrates the relationship between the propagation loss and arm width in the conventional slot waveguide. With the increase in arm width, the propagation loss starts to decrease. However, as mentioned in last sub-section, for G = 80 nm, the significant light confinement in slot region starts with W = 0.51 µm, and it reaches to maximum confinement at W = 0.52 µm. Correspondingly, the propagation loss starts to increase at W = 0.51 µm and reaches to maximum value at W = 0.52 µm and afterwards, it continuously decreases. Therefore, it can be predicted that in slot waveguides the high light confinement/EFR can be realized at the cost of high propagation loss. Moreover, to realize both low propagation loss and significant light confinement, the arm width must be chosen very judiciously, such as for G = 80 nm, at W = 0.55 µm, the EFR decreased by 3% only, while corresponding to this, there is significant decrement in propagation loss nearly by 7dB/cm in comparison with that at W = 0.52 µm. Similarly, for G = 120 nm, by choosing W = 0.56 µm, the reduction in EFR and corresponding propagation loss are respectively around 2.4% and 7.6 dB/cm in comparison to W = 0.54 µm.

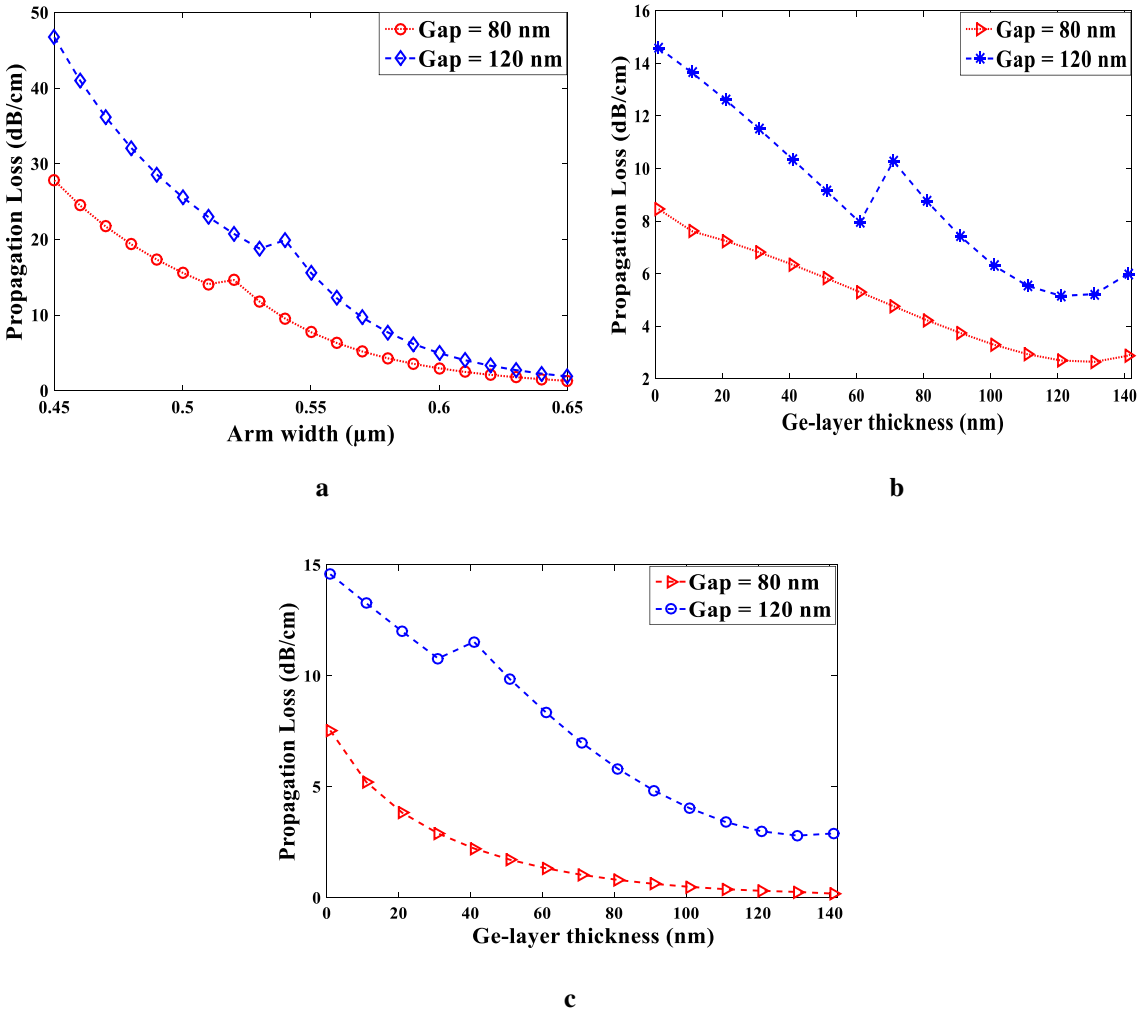

Fig. 6 Variations in propagation loss vs. **a** arm width (W) at two different slot gaps (G = 80 nm, and 120 nm) for slot waveguide **b** Ge-layer thickness (t) at two different slot gaps (G = 80 nm, and 120 nm) for partial-strip-loaded slot waveguide, and **c** thickness (t) at two different slot gaps (G = 80 nm, and 120 nm) for full-strip-loaded slot waveguide.

Moreover, for the analysis of propagation losses in partial-strip-loaded and full-strip-loaded slot waveguides, 'W' is again considered as 0.51 µm, and the Ge-layer thickness (t) has been varied up to 140 nm for the slot gaps of 80 nm, and 120 nm, as depicted in Figs. 6 **b** and **c** respectively. From the figures, it is clear that for G = 80 nm, the propagation loss continuously decreases with the increase in 't' without any jump in propagation loss at some mid value of 't', as observed with the G = 120 nm.

Similar to the previous analysis, the value of '*t*' must be chosen very carefully, to realize the significant EFR with low propagation loss. From Figs. 6, it has been observed that the propagation loss decreases with the increase in values of '*W*' and '*t*' and considerably less propagation loss can be recognized for the smaller slot gap. Moreover, from the propagation loss point of view, the performance of full-strip-loaded slot waveguide is quite better than that of the partial-strip-loaded slot waveguide, and appreciably superior than the conventional slot waveguide. Therefore, both partial-strip-loaded and full-strip-loaded slot waveguides can be suitably utilized for the design of the gas sensors based on the absorption of evanescent field.

3.4 Sensitivity variations for CH_4 gas sensor

By utilizing the Eq. (3), the values of sensitivity for all three slot waveguide structures have been estimated. The variations in sensing abilities with respect to the waveguide lengths have been depicted in Figs. 7 **a**, **b**, and **c** respectively for different EFR in slot region, propagation losses, and gas concentrations for all the three slot waveguides. For G = 80 nm, Fig. 7 **a** shows the nature of sensitivity variations for three different EFRs of 0.22, 0.27, and 0.28, that are obtained for the three respective slot waveguide structures, i.e., conventional slot, partial-strip-loaded slot, and full-strip-loaded slot waveguides, at a fixed propagation loss of 3 dB/cm.

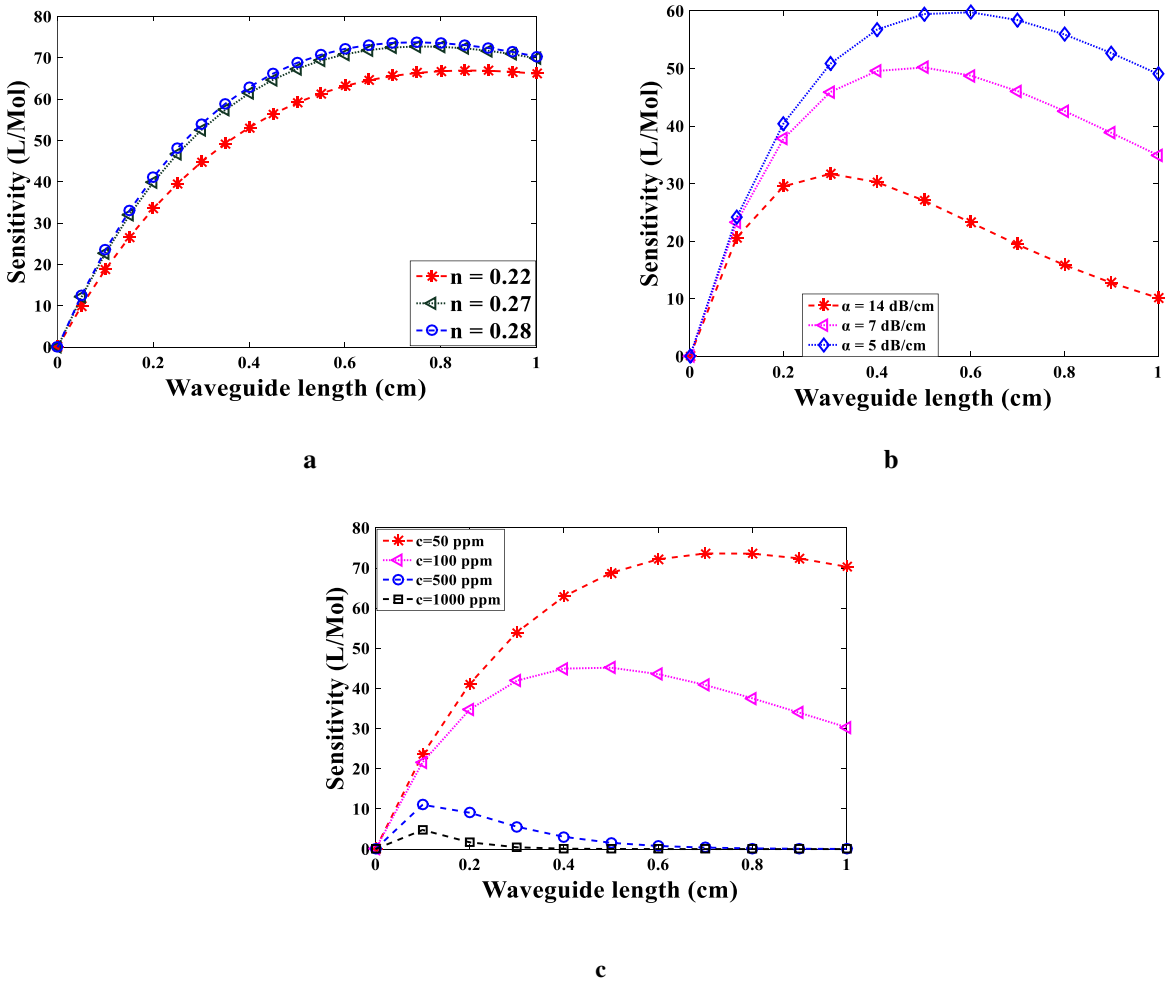

Fig. 7 Sensitivity vs. waveguide lengths for **a** three slot waveguide structures at their respective EFR values for fixed propagation loss of 3 dB/cm and G = 80 nm, **b** three slot waveguide structures at their respective EFR values for fixed EFR of 0.30 and G = 80 nm, and **c** four different methane gas concentrations for full-strip-loaded slot at G = 80 nm and EFR = 0.28.

The figure clearly depicts that the full-strip-loaded slot waveguide has the highest sensing ability, among the three structures. However, the variations in sensitivities of both partial-strip-loaded and full-strip-loaded slot waveguides are very close to each other, as their respective EFR values are very close, at the propagation loss of 3 dB/cm. Further,

the impact of variations in waveguide length have been illustrated in Fig. 7 **b** for different propagation losses of approximately 14 dB/cm, 7 dB/cm, and 5 dB/cm, realized respectively for conventional slot, partial-strip-loaded slot, and full-strip-loaded slot waveguides, for a fixed EFR of 0.30 and G = 80 nm. Under the considerations of the same EFR values for all the three slot waveguides, their propagation losses are different due to their specific design structures. Moreover, the partial-strip-loaded and conventional slot waveguides have reduced sensing abilities respectively by 5-15 L/Mol and 20-40 L/Mol, as compared to full-strip-loaded slot waveguide. This also recognizes the superiority of full-strip-loaded slot waveguide. Similarly, for different concentrations of methane gas, such as 50 ppm, 100 ppm, 500 ppm, and 1000 ppm, the variations in sensitivity have been analyzed in terms of waveguide lengths for full-strip-loaded slot waveguide and shown in Fig. 7 **c**. From the figure, it has been observed that with the increase in gas concentrations, the sensitivity decreases. However, for a particular gas concentration value, the sensitivity first increases, then at the optimum length it reaches to its maximum value and beyond this length, it starts to decrease.

4. Discussion and comparison

The conventional structure of the slot waveguides has been reported several times in the literature for different devices/applications. In the current work, the analysis of different slot waveguide structures based on Ge-on-CaF_2 materials have been explored, in order to search the possibilities to further enhance the performance of the slot waveguide in terms of evanescent field ratio, propagation loss, and sensitivity. The variations in evanescent field percentage in slot region have been realized by varying the arm widths (W) of slot waveguide. It has been observed that at W = 0.51 µm, the light confinement in slot region has started and it reaches to maximum at W = 0.52 µm, beyond that the light confinement/EFR decreases, for G = 80 nm. Based on this analysis and careful simulations with partial-strip-loaded and full-strip-loaded slot waveguides, their arm width has been fixed as 0.51 µm, and the variations in EFR have been observed by varying the Ge-layer thickness (t). The simulation results have exhibited that the significant light confinement (maximum EFR) can be achieved at some specific values of '*t'*, such as 60 nm and 40 nm, respectively for partial-strip-loaded and full-strip-loaded slot waveguides at G = 120 nm and beyond this value of '*t'*, the EFR decreases. However, it has also been observed that the high EFR/light confinement in slot region is always with the penalty in terms of high propagation loss. The low propagation loss is essentially required, in order to have light propagation for longer length as well as to achieve higher sensitivity. Therefore, to accomplish the significant EFR with low propagation loss, the values of '*W*' and '*t*' must be chosen very cautiously for all the considered waveguide structures. Further, the analysis of sensitivity variations has been carried out for a substantial range of waveguide lengths by varying the gas concentrations and waveguide parameters, such as EFR, and propagation loss. The higher sensitivities have been achieved with the higher EFR and lower values of gas concentration and propagation loss. Table 1 shows values of maximum achievable EFR and sensitivity for all the three slot waveguide structures for a relatively lower propagation loss of 3 dB/cm, and gas concentration of 50 ppm with G = 80 nm, and compared with the recently reported works.

Table 1: Comparison of obtained waveguide parameters for three slot waveguide structures at a fixed propagation loss of 3 dB/cm and gas concentration of 50 ppm.

Waveguide structures	α [dB/cm]	η (EFR)	Maximum Sensitivity (L/Mol)	Optimum waveguide length 'L_{opt}' (in cm)	Reference
Slot waveguide	3	0.22	66.93	0.86	This work (CH_4 sensor)
Partial-strip-loaded slot waveguide		0.27	72.50	0.762	
Full-strip-loaded slot waveguide		0.28	73.76	0.745	
Strip	2-5	0.10	-	-	2014 (Huang et al. 2014) (CO_2 sensor)
Rib	0.9-1.9	0.15	-	-	
Slot	~ 10	0.20	-	-	
Strip	3.98	0.14-0.16	-	-	2018 (Ranacher et al. 2018) (CH_4 sensor)
Strip	-	19.5	-	-	2018 (Ranacher et al. 2018) (CO_2 sensor)

As noted in Table 1, for the fixed value of waveguide propagation loss of 3 dB/cm, the highest EFR value can be realized as 0.28 for full-strip-loaded slot waveguide, which is closely followed by partial-strip-loaded slot waveguide with its corresponding EFR of 0.27. From the perspective of sensitivity, the highest sensitivity of 73.76 L/Mol can be realized with full-strip-loaded slot, which is pursued by partial-strip-loaded slot with sensitivity of 72.50 L/Mol. Moreover, the optimum waveguide length (L_{opt}) of conventional slot waveguide has the largest value, of 0.86 cm, among the three slot waveguide structures, and hence, the comparatively miniaturized photonic sensor can be realized with the full-strip-loaded and partial-strip-loaded slot waveguide structures. Therefore, Table 1 clearly validates the fact that the full-strip-loaded and partial-strip-loaded slot waveguides have reasonably better performance over the conventional slot waveguide. In general, the comprehensive analysis of this kind of sensors can be sorted into three parts namely, light source, sensing element, and photodetector. The current work mainly focused on the sensing element part for the light source having wavelength of 3.31 μm. However, photodetector is another important aspect for the design and analysis of photonic sensors. For the detection of light from these methane gas-sensing devices, the PbTe type of photodetector (Su et al. 2019) can be efficiently designed and used to detect the wavelength of 3.31 μm from the sensor device. This type of detector can provide the monolithic integration capability (i.e., integrated photodetectors), which makes it more reliable to detect the mid-IR lightwave.

5. Conclusion

In this work, the evanescent field absorption based methane gas sensor has been explored using three different slot waveguide structures, to investigate and increase the sensing capabilities of the photonic gas sensors. Among the three structures of waveguide, the partial-strip-loaded and full-strip-loaded slot waveguides have been realized by depositing the Ge-layer on CaF_2 in different ways, in anticipation of further improvement in sensing performance of the slot waveguides. The simulation analysis has been done by varying the arm width, and Ge-layer thickness, to achieve the efficient dimension of the waveguide structures. It has been observed that to achieve the high sensitivity, the higher EFR in slot region is required, which comes at the cost of higher propagation loss. Therefore, the dimension of slot waveguides must be chosen very judiciously to achieve the high EFR/sensitivity with significantly low propagation loss. The obtained results have depicted that full-strip-loaded slot waveguide has the highest EFR as well as highest sensitivity, which is closely followed by the partial-strip-loaded slot waveguide. Further, the detection of light from the sensor device is significant aspect for the comprehensive design and analysis of photonic sensors. Therefore, the current work can be extended for design and analysis of the efficient and reliable photodetector with high sensitivity, to increase the performance of the gas sensors.

Acknowledgments

The authors gratefully acknowledge National Institute of Technology Patna, and Science and Engineering Research Board, Department of Science and Technology, Government of India for providing COMSOL Multiphysics simulation software, used in the current simulation work.

References

Bogaerts, W., Baets, R., Dumon, P., Wiaux, V., Beckx, S., Taillaert, D., Luyssaert, B., Campenhout, J. V., Bienstman, P., and Thourhout, D. V.: Nanophotonic Waveguides in Silicon-On-Insulator Fabricated with CMOS Technology. Journal of Lightwave Technology 23 (1), 401 (2005)

Butt, M. A., Degtyarev, S. A., Khonina S. N., and Kazanskiy, N. L.: An evanescent field absorption gas sensor at mid-IR 3.39 μm wavelength. Journal of Modern Optics 64 (18), 1892-1897 (2017)

Ranacher, C., Consani, C., Vollert, N, Tortschanoff, A., Bergmeister, M., Grille, T., and Jakoby, B.: Characterization of Evanescent Field Gas Sensor Structures Based on Silicon Photonics. IEEE Photonics Journal 10 (5), 2700614 (2018)

Ranacher, C., Consani, C., Tortschanoffa, A., Jannesarib, R., Bergmeisterc, Grillec, M. T., and Jakoby, B.: Mid-infrared absorption gas sensing using a silicon strip waveguide. Sensors and Actuators A: Physical 277, 117–123 (2018)

Datta, A., Saha, A.: Manifestation of a highly sensitive evanescent wave absorption-based refractive index sensor realized by radiating with an optical Airy beam. Opt Quant Electron 53, 157 (2021)

Cherouana, A., Bencheikh, A. & Bouchama, I.: Effect of the electric field induced birefringence on the slab waveguide evanescent-wave sensor sensitivity. Opt Quant Electron 51, 331 (2019)

Butt, M. A., Khonina, S. N., and Kazanskiy, N. L.: Silicon on silicon dioxide slot waveguide evanescent field gas absorption sensor. Journal of Modern Optics 65 (2), 174-178 (2017)
Huang, Y., Kalyoncu, S. K., Zhao, Q., Torun, R., and Boyraz, O.: Silicon-on-sapphire waveguides design for mid-IR evanescent field absorption gas sensors. Optics Communications 313, 186-194 (2014)
Ding, R., Baehr-Jones, T., Kim, W. J., Xiong, X., Bojko, R., Fedeli, J. M.: Low-loss strip-loaded slot waveguides in silicon-on-insulator. Optics Express 18: 25061–25067 (2010)
Almeida, V. R., Xu, Q., Barrios, C. A., and Lipson A.: Guiding and confining light in void nanostructure. Optics Letter 29, 1209–1211 (2004)
Debnath, K., Khokhar, A. Z., Boden, S. A., Arimoto, H., Oo, S. Z., Chong, H. M., Reed, G. T., and Saito, S.: Low-loss slot waveguides with silicon (111) surfaces realized using anisotropic wet etching. Frontiers in Materials 3, 1-5 (2016)
Rifat, A. A., Ahmmed, R., and Bhowmik, B. B.: SOI Waveguide-Based Biochemical Sensors. Chapter 16,(2019)
Soref, R. A., Emelett, S. J., and Buchwald, W. R.: Silicon waveguided components for the long-wave infrared region. Journal of Optics A: Pure and Applied Optics 8 (10), 840 (2006)
Tien, E., Huang, Y., Gao, S., Song, Q., Qian, F., Kalyoncu, S. K., and Boyraz, O.: Discrete parametric band conversion in silicon for mid-infrared applications. Optics Express 18, 21981-21989 (2010)
Baehr-Jones, T., Spott, A., Ilic, R., Spott, A., Penkov, B., Asher, W., and Hochberg, M.: Silicon-on-sapphire integrated waveguides for the mid-infrared. Optics Express 18, 12127-12135 (2010)
Li, F., Jackson, S. D., Grillet, C., Magi, E., Hudson, D., Madden, S. J., Moghe, Y., Brien, C. O., Read, A., Duvall, S. G., Atanackovic, P., Eggleton, B., and Moss, D.: Low propagation loss silicon-on-sapphire waveguides for the mid-infrared. Optics Express 19: 15212-15220 (2011)
Xu, Y., Li, J., Kong, M. et al.: Bent silicon slot waveguides with both low loss and low nonlinearity. Opt Quant Electron 52, 445 (2020)
Nacer, S., Aissat, A.: Optical sensing by silicon slot-based directional couplers. Opt Quant Electron 44, 35–43 (2012)
Parriaux, O., and Veldhuis, G. J.: Normalized analysis for the sensitivity optimization of integrated optical evanescent-wave sensors. Journal of Lightwave Technology 16 (4), 573–582 (1998)
Kai-he, X., Xin, Z., Xiao-wei, Z., Han, Jin., and Jia-wen, J.: A slot microring sensor with feedback spiral waveguide for trace gas CH4 sensing in mid-infrared region. Optoelectronics Letters 15 (1), 1-5 (2019)
Mere, V., and Selvaraja, S. K.: Germanium-on-Glass waveguides for Mid-IR photonics. 13th International Conference on Fiber Optics and Photonics. OSA Technical Digest, Optical Society of America (2016)
Soref, R.: Mid-infrared photonics in silicon and germanium. Nature Photonics 4, 495-497 (2010)
Kim, S., Han, J., Shim, J., Kim, H., and Choi, W. J.: Verification of Ge-on-insulator structure for a mid-infrared photonics platform, Optical Materials Express 8 (2), 440-451 (2018)
Dong, M., Zheng, C., Miao, S., Zhang, Y., Du, Q., Wang, Y., Tittel, F.K.: Development and Measurements of a Mid-Infrared Multi-Gas Sensor System for CO, CO2 and CH4 Detection. Sensors 17, 2221 (2017)
Zheng, H., Lou, M., Dong, L., Wu, H., Ye, W., Yin, X., Kim, C. S., Kim, M., Bewley, W., Merritt, C. D., Canedy, C. L., Warren, M. V., Vurgaftman, I., Meyer, J. R., and Tittel, F. K.: Compact photoacoustic module for methane detection incorporating interband cascade light emitting device. Optics Express 25, 16761-16770 (2017)
Rouxel, J., Coutard, J. G., Gidon, S., Lartigue, Nicoletti, O., Parvitte, S. B., Vallon, R., Zeninari, V., Gliere, A.: Development of a Miniaturized Differential Photoacoustic Gas Sensor. Procedia Engineering 120, 396-399 (2015)
Fabricius, N., Gauglitz, G., and Ingenhoff, J.: A gas sensor based on an integrated optical Mach-Zehnder interferometer. Sensors and Actuators B: Chemical 7, 672-676 (1992)
Yebo, N. A., Lommens, P., Hens, Z., and Baets, R.: An integrated optic ethanol vapor sensor based on a silicon-on-insulator microring resonator coated with a porous ZnO film. Optics Express 18, 11859-11866 (2010)
Katti, R., Prince, S.: Photonic Delay Lines Based on Silicon Coupled Resonator Optical Waveguide Structures. Silicon 10, 2793–2800 (2018)
Chandra, V., Ranjan, R.: Performance analysis of slot waveguide using aluminum nitride in slot region. Opt Quant Electron 52, 231 (2020)
Du, W., Chen, Z. B., and Zhao, F.: Analysis of single-mode optical rib waveguide in silicon carbide. Microwave Optical Technology Letter 55 (11), 2636–2640 (2013)
Lindecrantz, S. M., and Helles, O. G.: Estimation of Propagation Losses for Narrow Strip and Rib Waveguides. IEEE Photonics Technology Letters 26 (18), 1836-1839 (2014)
Huang, H. K., Liu, B. Qi, and Sorger, V. J.: Re-analysis of single-mode conditions for silicon Rib waveguides at 1550 nm wavelength. Journal of Lightwave Technology 34 (16), 3811-3817(2016)
Lio, Y., Kong, M., and Jiang, Y.: Transverse magnetic modes in planar slot waveguides. Journal of the Optical Society of America B 32 (10), 2052-2060 (2015)
Verma, A., Prakash, A. and Tripathi, R.: Comparative study of a Surface Plasmon Resonance Biosensor based on Metamaterial and Graphene. Silicon 9, 309–320 (2017)
Ranacher, C. et al.: Mid-infrared absorption gas sensing using a silicon strip waveguide. Sens. Actuators A, Phys. 277, 117–123 (2018)
Su, P., Han, Z., Kita, D., Becla, P., Lin, H., Deckoff-Jones, S., Richardson, K., Kimerling, L. C., Hu, J., and Agarwal, A.: Monolithic on-chip mid-IR methane gas sensor with waveguide-integrated detector. Applied Physics Letter 114, 051103 (2019).

Figures

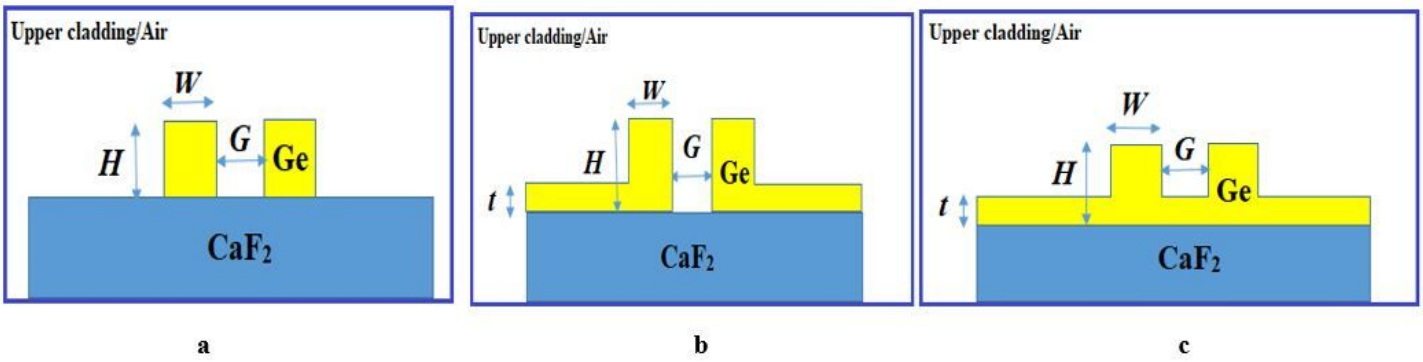

Figure 1

Structures of three different slot waveguides using Ge-on-CaF2 materials a conventional slot waveguide, b partial-strip-loaded slot, and c full-strip-loaded slot.

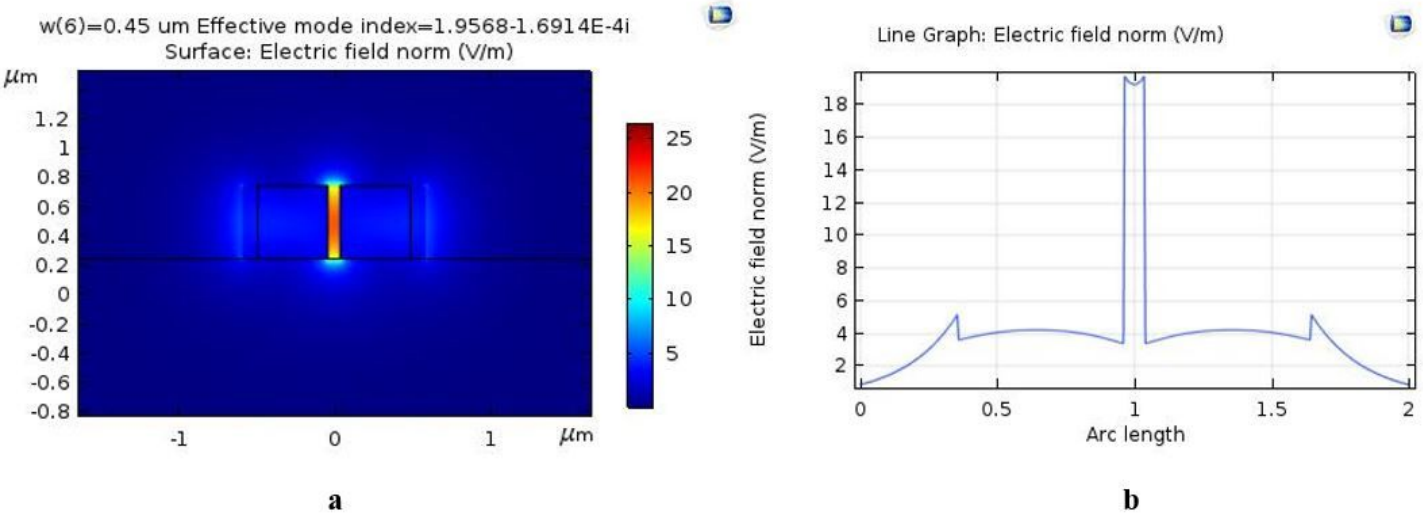

Figure 2

Mode field distribution for a conventional slot waveguide, and b plot of corresponding normalized electric field distribution at W = 0.55 μm, G = 0.08 μm, and H = 0.50 μm.

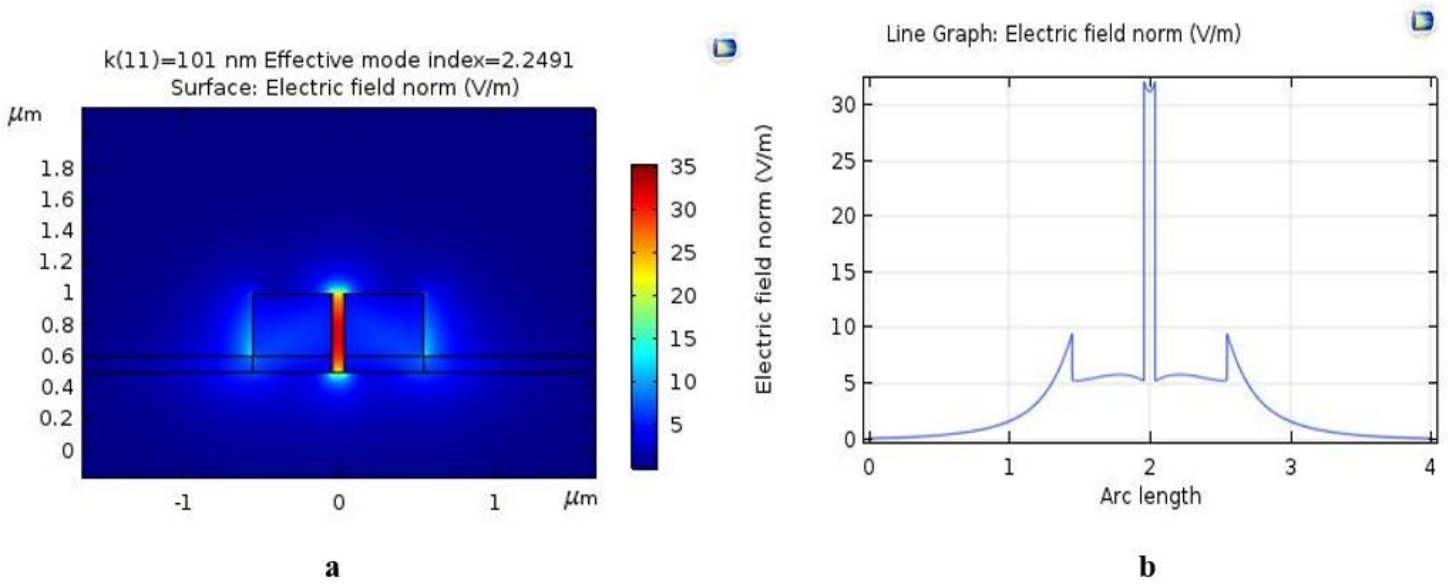

Figure 3

Mode field distribution for a partial-strip-loaded slot, and b plot of corresponding normalized electric field distribution (right) at W = 0.51 μm, G = 80 nm, H = 0.5 μm, and t = 101 nm

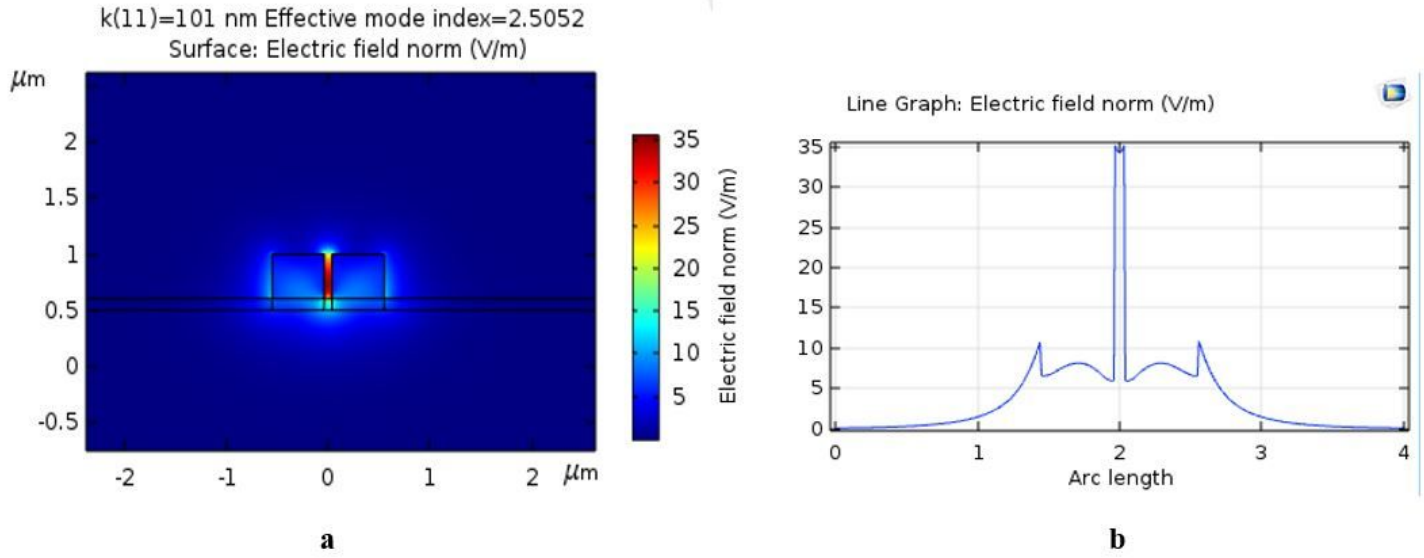

Figure 4

Mode field distribution a for full-strip-loaded slot, and b plot of corresponding normalized electric field distribution at W = 0.51 μm, G = 80 nm, H = 0.5 μm, and t = 101 nm.

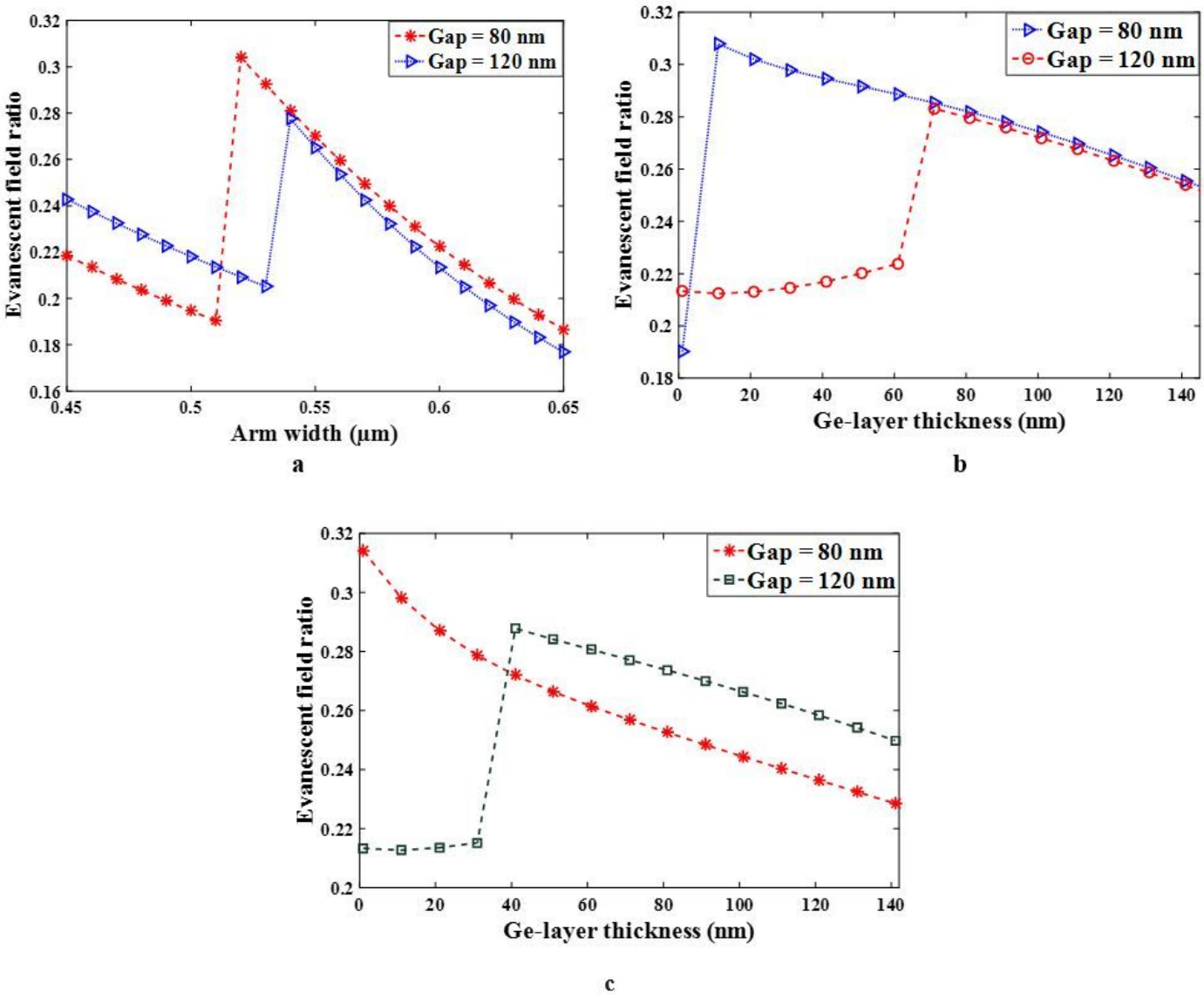

Figure 5

Evanescent field ratio variations a with the arm width (W) at two different slot gaps (G) in Slot waveguide b with Ge-layer thickness (t) at two different slot gaps (G) in partial-strip-loaded slot, and c with Ge-layer thickness (t) at two different slot gaps (G) in full-strip-loaded slot waveguide.

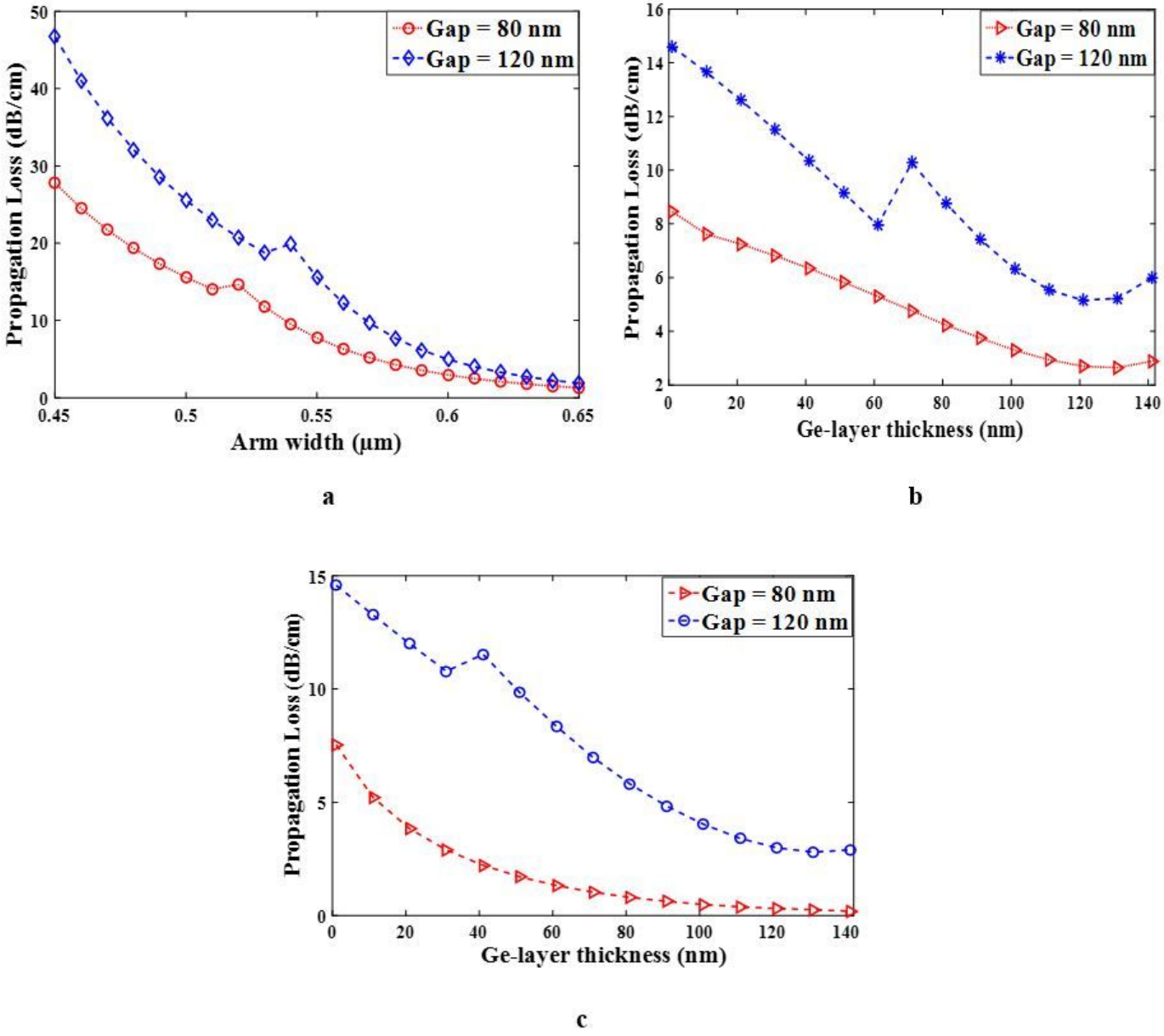

Figure 6

Variations in propagation loss vs. a arm width (W) at two different slot gaps (G = 80 nm, and 120 nm) for slot waveguide b Ge-layer thickness (t) at two different slot gaps (G = 80 nm, and 120 nm) for partial-strip-loaded slot waveguide, and c thickness (t) at two different slot gaps (G = 80 nm, and 120 nm) for full-strip-loaded slot waveguide.

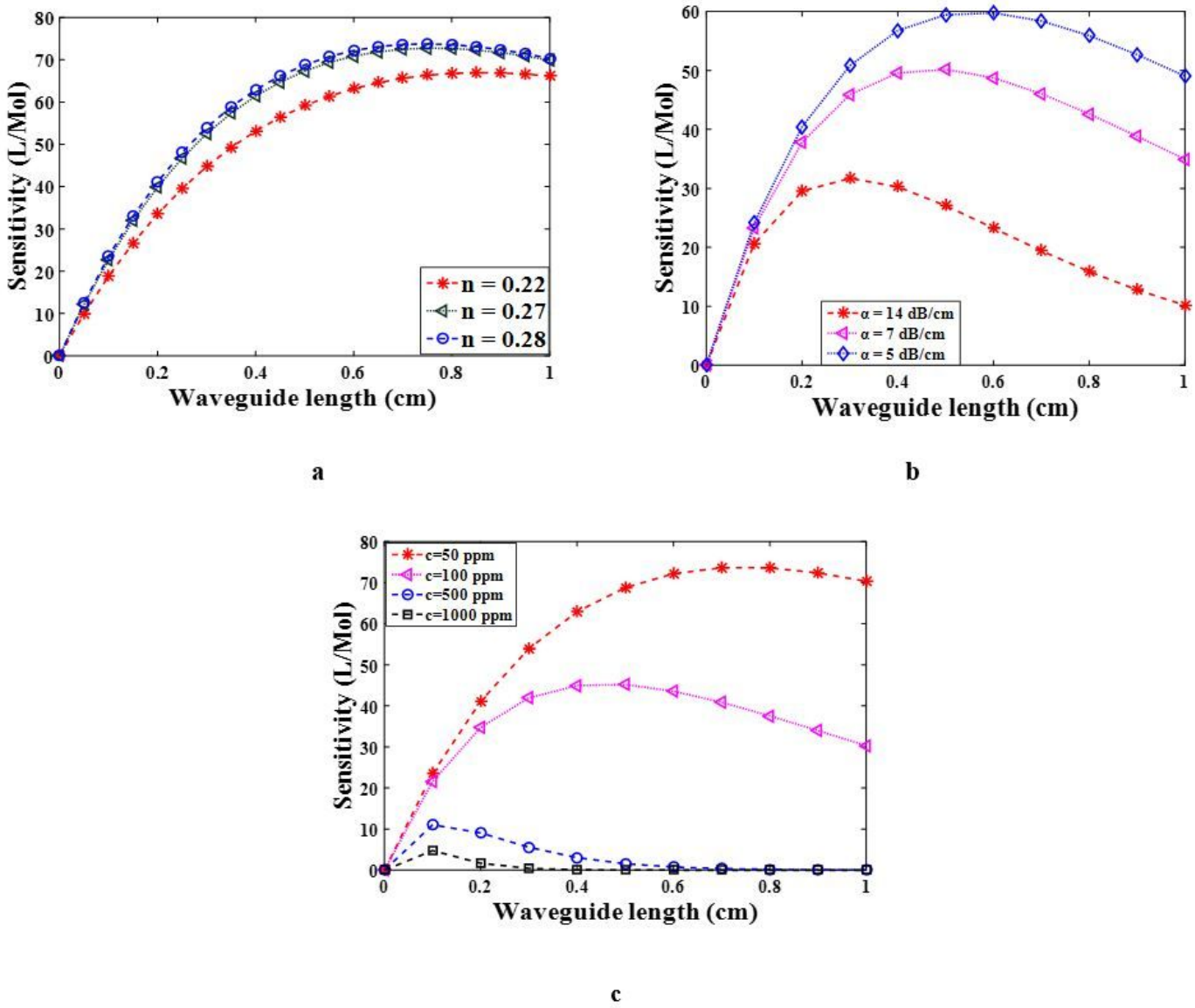

Figure 7

Sensitivity vs. waveguide lengths for a three slot waveguide structures at their respective EFR values for fixed propagation loss of 3 dB/cm and G = 80 nm, b three slot waveguide structures at their respective EFR values for fixed EFR of 0.30 and G = 80 nm, and c four different methane gas concentrations for full-strip-loaded slot at G = 80 nm and EFR = 0.28.